Materials Research. 2018; 21(3): e20170715
DOI: http://dx.doi.org/10.1590/1980-5373-MR-2017-0715

Investigation on Friction and Wear Properties of High-Temperature Bearing Steel 9Cr18Mo

Qiang He[a,b], Anling Li[a], Wenhong Qu[c], Yong Zhang[a], Tao Wang[a], Linghao Kong[a]*

[a]*Department of Mechanical Engineering, Anyang Institute of Technology, Anyang, China*
[b]*Department of Mechanical Engineering,University of South Carolina,Columbia,USA*
[c]*Quality and Technical Supervision Testing Center of Anyang, 455000, China*

Received: August 07, 2017; Revised: January 27, 2018; Accepted: March 01, 2018

This paper presented a study of friction and wear on 9Cr18Mo when rubbed against other materials (steel-304, steel-440C, steel-GCr15 or silicon nitride ceramic ball) at high temperature conditions. Friction and wear tests were carried out with universal a friction and wear testing machine. The wear morphology was analyzed by a Nanovea three-dimensional profilometer and trinocular positive Gang metallurgical microscope. The Vickers hardness of 9Cr18Mo at different temperatures was tested by means of a high temperature vacuum hardometer. Results showed that the friction and wear on the contact surface of the 9Cr18Mo sample are higher when the hardness of counter materials is higher than or similar to that of the sample. Under dry sliding conditions, the 9Cr18Mo sample surface presented various degrees of adhesion, plowing and pit, particularly if tested in the presence of a high temperature environment. During the worn stages, the counter materials on the worn surface successively produced cracks, crack growth, and wear debris under the action of load. Moreover, the frictional pair 9Cr18Mo-ceramic showed good anti-wear behavior at 400 °C that proved the anti high temperature performance of 9Cr18Mo.

Keywords: *9Cr18Mo, Wear morphology, Friction and wear, counter materials.*

1. Introduction

To ensure the reliability and stability of high-speed bearings, the bearing steel must possess high hardness, high temperature resistance, wear resistance, fracture toughness, dimensional stability, and corrosion resistance.[1-5] Due to its good mechanical properties and corrosion resistance, 9Cr18Mo (AISI 440C) martensitic stainless steel is widely used as a bearing material in energy, aerospace, metallurgy, materials processing, and other industrial fields.[6-8] However, the long operation time of bearings materials will produce pitting and wear on the surfaces leading to the failure of bearings and abnormal operation of devices.[9-12] Moreover, the degraded performance of vulnerable parts in mechanical products is mostly caused by friction and wear. If the amount of unnecessary friction and wear can be reduced and controlled, the performance and service life of vulnerable parts will be improved. Therefore, the understanding of the friction and wear mechanisms is of great significance on the improvement of reliability and stability of bearings.[13-21]

In harsh conditions, a conventional lubrication of moving parts is difficult. These moving parts typically operate under dry conditions such as in dust and sand. Therefore, the investigation of the tribological characteristics of engineering materials under dry sliding conditions is necessary.[22-25] Ma et al.[26] researched the friction and wear behaviour of steel with bionic non-smooth surfaces under dry wear condition, and results showed that the bionic surface of testing samples had better wear resistance and provided stable friction coefficient to some extent. Sun et al.[27] studied the sliding wear behavior of plasma nitrided layers produced in AISI 316 type austenitic stainless steel at high temperatures. The results indicated that the plasma nitriding at various temperatures increases the wear resistance of 316 steel by more than two orders of magnitude when sliding against bearing steel under dry sliding conditions. Jin et al.[28] reasearched the tribological properties of bronze-Cr-Ag composites sliding against AISI 52100 steel under dry sliding conditions. Thus, various studies indicated the importance of friction and wear behavior of bearing steel under dry sliding conditions.

High temperature friction involves energy transfer, material migration and transformation between two frictional surfaces. Such transformation mainly involves adhesion, plowing, deformation between two relative motion surfaces and damage, and loss of material. At high speeds and high temperature environments, the temperature of the frictional surface is extremely high leading to oxidation, phase change and composition change. The frictional properties of materials will be influenced by these variations.

The ceramic, steel-440C, steel-GCr15 and steel-304 is the most commonly used as bearing material. The inner and outer ring of some high-temperature bearings is steel, but the ball is ceramic. Therefore, we study the friction properties of several bearing materials with different temperature have practical significance. In this paper, to investigate the tribological properties of 9Cr18Mo bearing steel, the performance tests of 9Cr18Mo was completed. At room temperature and high temperature conditions,

*e-mail: aystar@163.com

the coefficient of friction and worn surface for 9Cr18Mo sample were analyzed by changing its frictional pair (steel-304, steel-440C, steel-GCr15, or silicon nitride ceramic).

2. Materials and Experimental Method

The experimental methodology basically consisted of rubbing spherical pellets on the top surface of a metallic cylinder-shaped sample (i.e. the cylinder-shaped sample and the pellets constitute frictional pairs). While the material of the cylinder-shaped sample, here and after call "the sample", was the same over all the experiments, the material of the pellets was varied. Therefore, the samples are considered the basic frictional pair, and the pellets are considered the secondary frictional pair. The next subsections describe the materials used and the experimental methodology followed to investigate the characteristics of wear and friction on the basic frictional pair as the secondary frictional pair is varied.

2.1 Preparation of test materials

The basic frictional pair was made of 9Cr18Mo bearing steel. The chemical composition of the 9Cr18Mo sample was measured by Foundry-Master Pro vertical direct reading spectrometer (see Table 1). The secondary frictional pair (pellets 6 mm in diameter) was made of silicon nitride ceramic, steel-440C, steel-GCr15, or steel-304.

Fig. 1 shows a mechanical drawing of the basic frictional pair sample for the room temperature friction and wear test. These samples were fabricated in accordance with the requirements of the testing machine. Before conducting friction and wear tests, it was determined the variation of the sample hardness during temperature changes was determined. The 9Cr18Mo sample size for the high temperature Vickers hardness tests was ϕ40×10 mm. Finally, high temperature reciprocating friction and wear tests were performed in one frictional pair (9Cr18Mo-ceramic) by varying the temperature in order to investigate the effects of high temperatures on the severity of friction and wear. The sample size for the high temperature reciprocating friction and wear tests was ϕ12×3 mm.

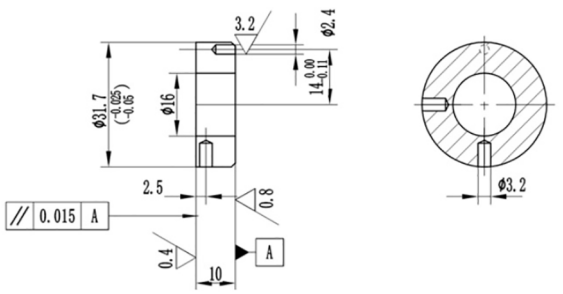

Figure 1. Mechanical drawing for the friction and wear of 9Cr18Mo samples

2.2 Experimental method

The experimental methodology consisted of successively performing the next experimental tests: high temperature Vickers hardness test, friction and wear test at room temperature, and friction and wear test at high temperature. These tests can be described as follows:

(1) High temperature Vickers hardness test. This test was carried out with a HVT-1000W high-temperature vacuum hardometer which can provide 2×10^{-5} Pa of vacuum degree. Tests were conducted at different sample temperatures (20, 100, 200, 300 and 400 °C) with a normal load of 10 N and a dwell time of 30 s. The varied temperatures are provided by the heating module and maintained steadily through the temperature control sensor in the hardometer. Since the suitable operating temperature for 9Cr18Mo bearing steel should be below 380 °C, no temperatures exceeding 400 °C were investigated in this experimental research.

(2) Room temperature friction and wear test. This test was conducted on a MMW-1A universal friction and wear testing machine (see Fig. 2(a)). This testing machine is controlled by a computer and the working principle of the tests is shown in Fig. 2(b). The worn morphology of the sample was observed by a trinocular positive Gang metallurgical microscope and its weight loss was measured by means of an electronic balance. Several tests were conducted by varying the pellets rubbing against the 9Cr18Mo sample and by keeping a rotational speed of 100 rev/min, a load of 20 N, and a period of 5 min.

(3) High temperature reciprocating friction and wear test. This test was conducted on a MGG-02 high temperature reciprocating friction and wear testing machine (observe Fig. 3(a)). The working principle of the high temperature reciprocating friction and wear test is shown in Fig. 3(b). With the same load and testing time, the friction coefficient for 9Cr18Mo-cermaic frictional pair at different temperatures (20, 100, 200, 300 and 400 °C) was evaluated. These experiments were performed with a load of 20 N, stroke of 2 mm, frequency of 20 Hz, and period of 5 min. The surface roughness and the three-dimensional morphology of the sample, before and after the test, were observed by means of a 3D profilometer. The amount and volume of wear were determined by the wear measuring instrument.

Table 1. Chemical composition of 9Cr18Mo bearing steel.

Element	C	Si	Mn	P	S	Cr	Mo	Ni
Content (wt.%)	0.974	0.008	0.498	0.019	0.005	17.2	0.492	0.092

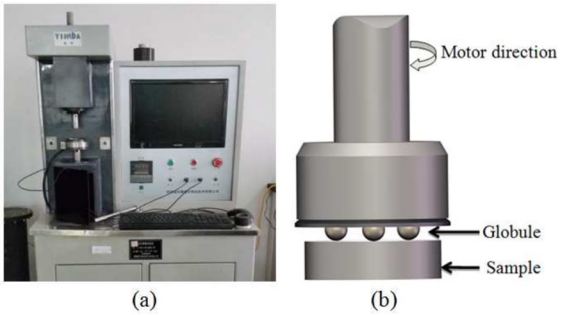

Figure 2. MMW-1A universal friction and wear testing machine: (a) experimental setup and (b) working principle

3. Results and Discussion

3.1 High temperature Vickers hardness test

The Vickers hardness (HV) of the bearing steel 9Cr18Mo sample at different temperatures was obtained with a load of 10 N and a period of 30 s. The resultant indentations under different temperatures are shown in Fig. 4. The Vickers hardness was calculated according to the next equation:

$$HV = 0.102 \times \frac{F}{S} = 0.102 \times \frac{2F\sin\frac{\alpha}{2}}{d^2} \quad (1)$$

Figure 3. MGG-02 high temperature reciprocating friction and wear testing machine: (a) experimental setup and (b) working principle

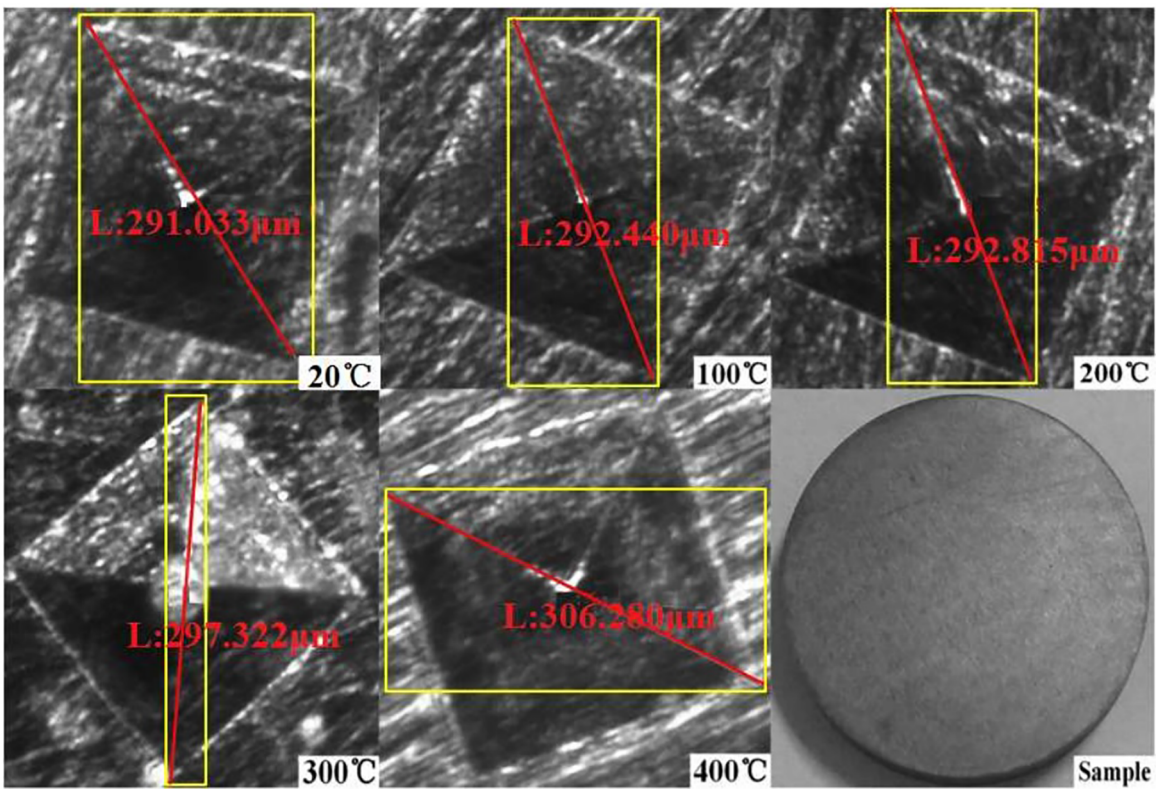

Figure 4. The sample indentations under different temperatures. Note: the red diagonals are the diagonal length of mean indentation (*d*)

Where F is the load (N), S is the indentation area (mm^2), α is the head relative angle (136°), and d is the diagonal length (mm)of mean indentation.

Fig. 5 shows the variation of the hardness of the 9Cr18Mo sample bearing steel with increasing temperature. As shown in the figure, the Vickers hardness of 9Cr18Mo decreases rapidly with increasing temperature, especially when increasing from room temperature to 200 °C. It is important to mention that the resistance value and oxidation degree of the sample surface could have a significant impact on the test results. Therefore, the vacuum degree inside the vacuum chamber was the same during any test, and the vacuum pump was turned off until the samples cooled down to the same temperature after the end of the test.

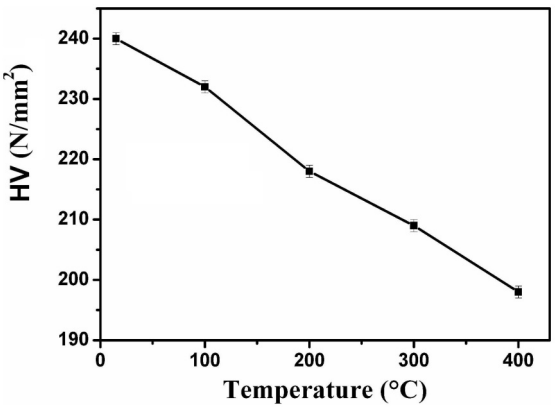

Figure 5. The variation of the hardness of the 9Cr18Mo sample with increasing temperature

3.2 Analysis of room temperature friction and wear test

Fig. 6 shows the temporal variation of the friction coefficient of 9Cr18Mo with different secondary frictional pairs. The friction coefficient curves for 9Cr18Mo-ceramic and 9Cr18Mo-GCr15 grow over time. Although the coefficient of friction curve for 9Cr18Mo-ceramic shows a decrease on the last few 25 s of the test. the friction coefficient curve for 9Cr18Mo-440C monotonically increases over time with exception of two short time intervals of the test (50-100 s and 275-300 s). The only friction coefficient curve showing significant fluctuations is the one for 9Cr18Mo-304 which approximately fluctuates from 0.5 to 0.6. The 9Cr18Mo-ceramic, 9Cr18Mo-440C and 9Cr18Mo-GCr15 frictional pairs show similar temporal coefficient of friction behavior, but that of the 9Cr18Mo-304 frictional pairs is quite different. The friction coefficient for 9Cr18Mo-304 frictional pair was larger than the others in most of the test time.

The 3D profilometer was used to observe the worst part of the local wear. From the observed results, the friction and wear properties of the 9Cr18Mo samples with secondary frictional pairs were analyzed. The worn morphologies for the 9Cr18Mo sample with different secondary frictional pairs are given in Fig. 7. As shown in the figure, the frictional surfaces have different degrees of abrasion and binding under dry friction state. The wear marks are significantly severe. In theory, the temperature of the contact surface was higher than other regions during the test, therefore the contact surface as the worn surface could easily produce cracks, crack growth and wear debris. This transition from mild to severe wear was mainly due to the effect of the temperature on the structure properties of 9Cr18Mo samples as the temperature increases.

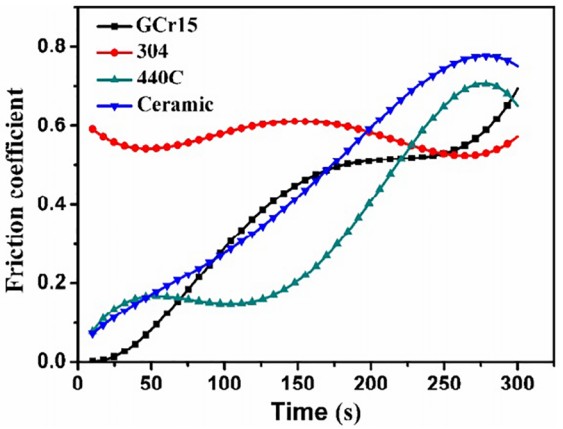

Figure 6. The variation of the friction coefficient for 9Cr18Mo and different secondary frictional pairs

The mass of the 9Cr18Mo sample before and after the test was measured by an electronic balance in precision. Fig. 8 shows the weight loss of the 9Cr18Mo sample in function of the frictional pair used. The rate of wear volume was calculated according to the next equation:

$$W = \frac{V}{N \times L} = \frac{\Delta m}{\rho \times N \times 2\pi r \times \nu \times t} \qquad (2)$$

Where V is the worn volume, N is the test load, L is the friction distance, Δm is the worn mass, ρ is the actual density of the sample, r is the friction radius, v is the frictional rotational speed and t is the frictional time. The largest and smallest weight losses were obtained for the 9Cr18Mo-440C and the 9Cr18Mo-ceramic frictional pairs, respectively. These results indicate that the friction and wear on the contact surface of the 9Cr18Mo sample are higher when the hardness of the secondary frictional pair is higher than or similar to that of the sample. Additionally, the worn width and weight loss of the 9Cr18Mo sample were greatly influenced by the coefficient of friction. The 9Cr18Mo-304 frictional pair with the largest coefficient of friction had the worst worn surface.

In order to identify the degree of friction and wear, it is indispensable to investigate the worn morphology

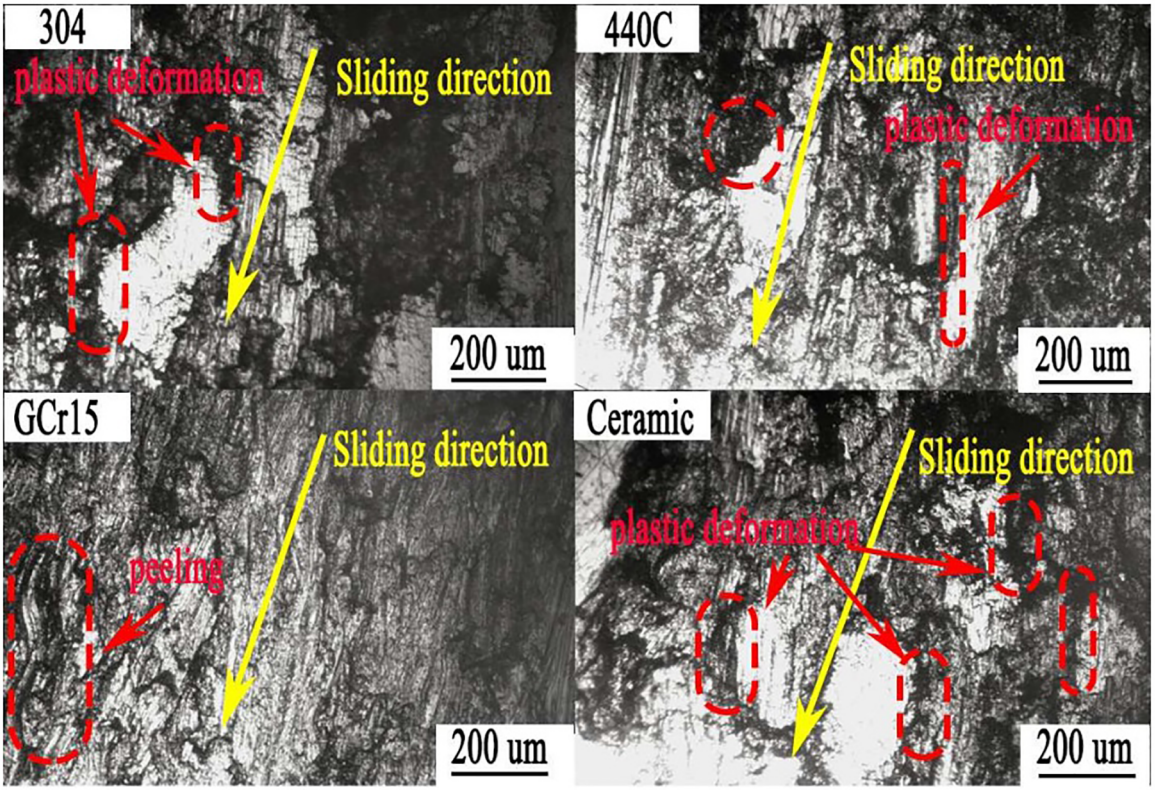

Figure 7. Worn morphologies for 9Cr18Mo with different secondary frictional pairs

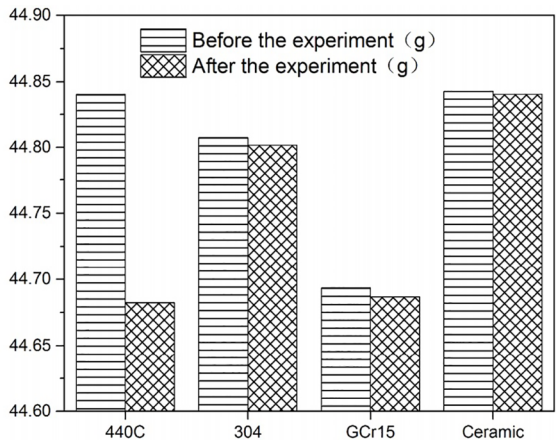

Figure 8. The mass of the 9Cr18Mo sample before and after the tests

of different friction pairs. Fig. 9 shows the stereogram and depth image of grinding cracks from four different friction pairs. Components of each pair were rubbed against each other under same conditions, and the results were measured by three dimension profilometer. We can see from the three-dimensional topography, the wear of 440C steel is more serious, the wear scar is wide and deep. The wear of ceramic is lighter, the wear scar is relatively narrow and shallow.

Through analysis and calculation, the wear surface parameters of the 9Cr18Mo sample after being rubbed against the different balls were determined (see Table 2). The deepest point and sectional view of grinding marks on each 9Cr18Mo sample are shown in Fig. 10. At the dry frictional state, the frictional wear surface had varying degrees of burning, adhesion, plowing and pit for the different secondary frictional pairs. The pit depth was deeper in the 9Cr18Mo-304 and 9Cr18Mo-GCr15 frictional pairs, because these frictional pairs presented higher coefficients of friction.

3.3 Analysis of high temperatures friction and wear test

Because the good performance of 9Cr18Mo-ceramic frictional pair at room temperature friction and wear test, it is necessary to investigate the friction and wear behaviors of 9Cr18Mo-ceramic pair at high temperatures. The surface roughness, coefficient of friction, as well as worn volume were determined before and after each test (see Table 3). Additionally, the deepest points and sectional views for each test were generated too (see Fig. 11). At the dry friction state, the frictional surface had varying degrees of adhesion, plowing and pit at different temperatures. The pit depth was deeper with increasing temperature. This transition demonstrated that the temperature highly acted on the structure properties of 9Cr18Mo sample.

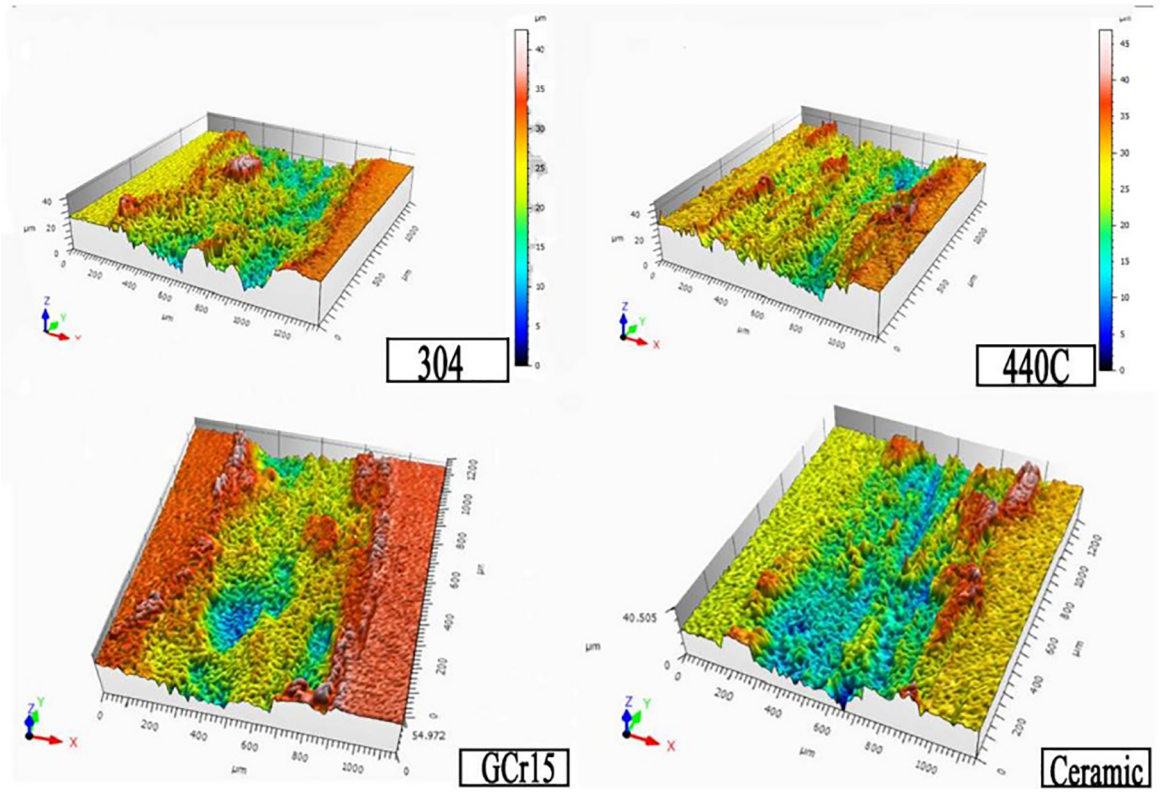

Figure 9. Three-dimensional wear morphology of four kinds of materials

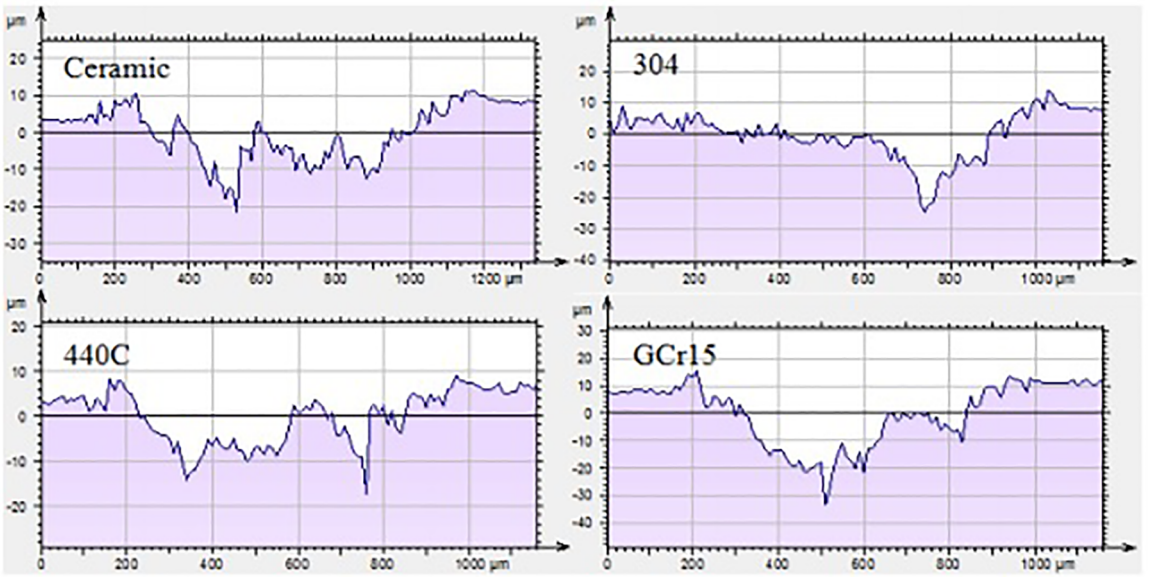

Figure 10. The deepest point and sectional view of the grinding marks on the 9Cr18Mo sample surface for different frictional pairs

Table 2. The worn surface parameters for the 9Cr18Mo sample in function of the secondary frictional pair.

Parameter (μm)	Ceramic	Steel-304	Steel-440C	Steel-GCr15
Largest wave height	19.200	19.989	19.781	18.643
Largest sag height	23.338	26.909	20.076	36.329
Maximum altitude	42.538	46.898	39.857	54.972
Arithmetic average height	4.743	4.466	4.934	7.205
RMS height	5.835	5.643	6.064	8.543

Table 3. The friction and wear experimental data for the 9Cr18Mo sample when rubbed by the ceramic frictional pair.

Experimental temperature (°C)	20	100	200	300	400
Surface roughness before test (μm)	0.822	0.782	0.761	0.813	0.807
Surface roughness after test (μm)	3.125	2.916	2.972	3.207	2.813
Friction coefficient	0.1497	0.1524	0.1613	0.1951	0.1568
Worn volume (mm^3)	0.0049	0.0056	0.0082	0.0131	0.0072

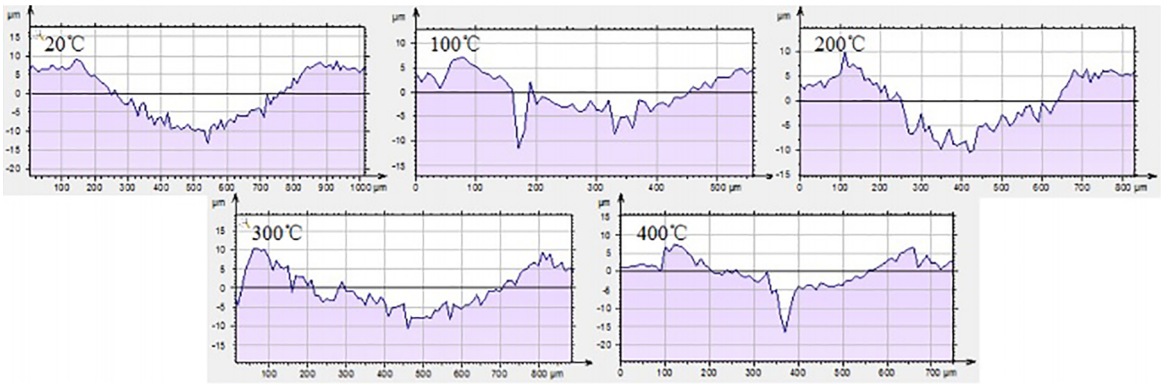

Figure 11. The deepest point and sectional view of the grinding marks on the 9Cr18Mo sample surface for the ceramic frictional pair and at different test temperatures

Fig. 12 shows the variation of the friction coefficient and worn volume as functions of temperature for the 9Cr18Mo sample when rubbed by the ceramic frictional pair. By comparison, it can be seen that the high temperature friction and wear properties of the 9Cr18Mo sample are the worst at 300 °C. And the 9Cr18Mo-ceramic frictional pair show good friction and wear behaviors at 400 °C. It is possible that the formation of protective film on the worn surface at 400 °C leads to the decrease of friction coefficient.

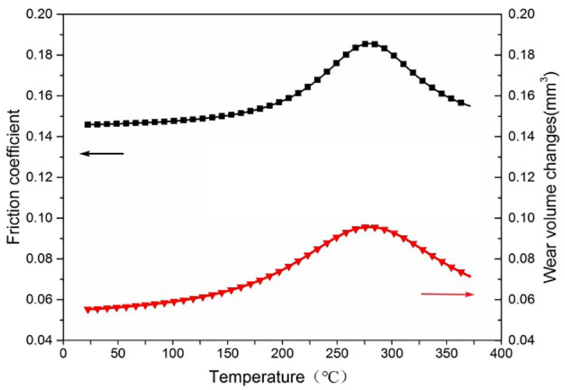

Figure 12. The coefficient of friction and worn volume for the 9Cr18Mo sample as functions of temperature

4. Conclusions

In this paper, to investigate the tribological properties of 9Cr18Mo bearing steel, the performance tests of 9Cr18Mo and the frictional and wear experiments for 9Cr18Mo paired to different frictional pairs were performed. The Vickers hardness and friction coefficients were evaluated. The worn surfaces, weight loss, and worn volume of the 9Cr18Mo samples were analyzed. The following conclusions resulting from the tribological experiments can be derived:

1. The Vickers hardness of 9Cr18Mo was determined to decrease rapidly with increasing temperature, especially from room temperature to 200 °C.
2. The friction and wear on the contact surface was found to be higher when the 9Cr18Mo sample was rubbed against the 440C-ball because of the similar hardness. The transition from mild wear to severe wear was due to the effect of the temperature on the structure properties of 9Cr18Mo sample, so the friction and wear of the frictional surface at high temperatures was higher. Moreover, the frictional pair 9Cr18Mo-ceramic showed good anti-wear behavior at 400 °C.

5. Acknowledgements

This research project was supported by the National Natural Science Foundation of China (51105002), the National Science and Technology Major Project (2012ZX04005-021), the Natural Science Foundation of the Henan Province (152102210196), and the Foundation of the Henan Educational Committee (16A460001).

6. References

1. Sourmail T, Millot-Méheux M. Thermal and mechanical stability of retained austenite in 1%C bearing steels with varying Si contents. *Materials Science and Technology*. 2016;32(11):1126-1132.

2. Li YJ, Herbig M, Goto S, Raabe D. Formation of nanosized grain structure in martensitic 100Cr6 bearing steels upon rolling contact loading studied by atom probe tomography. *Materials Science and Technology*. 2016;32(11):1100-1105.

3. Pei YT, Galvan D, De Hosson JTM, Cavaleiro A. Nanostructured TiC/a-C coatings for low friction and wear resistant applications. *Surface and Coatings Technology*. 2005;198(1-3):44-50.

4. Yan WK, Yang MS, Du JH, Yu F. Microstructure Evolution and Rapid Spheroidizing Technology of High-Purity of GCr15 Bearing Steel. *Iron & Steel*. 2010;45(12):63-67.

5. Sun HY, He Q, Zhou ZJ, Wang M, Zhang GM, Li SF. Effects of Solution Depletion and Segregation Oxidation on Morphology of Modified 310 Austenitic Stainless Steel. *Journal of Iron and Steel Research, International*. 2016;23(4):393-400.

6. Zeng ZM, Zhang T, Tian XB, Tang BY, Kwok TK, Chu PK. Surface modification of 9Cr18 bearing steels by a metal and carbon co-plasma immersion ion implantation. *Surface and Coatings Technology*. 2000;128-129:236-239.

7. Liu F, Fu G, Cui Y, Sun Q, Qu M, Sun Y. Tribological properties and surface structures of ion implanted 9Cr18Mo stainless steels. *Nuclear Instruments and Methods in Physics Research Section B: Beam Interactions with Materials and Atoms*. 2013;307:412-418.

8. Liu F, Li J, Jin J, Zhou G, Qiu W, Qing T. Surface Structures and Mechanical Properties of 9Cr18Mo Stainless Steels Implanted with Nitrogen Ions. *Rare Metal Materials & Engineering*. 2013;42(9):1838-1843.

9. Davim JP. Tribology of Composite Materials. *Journal of the Japan Society for Composite Materials*. 1985;25(2):148.

10. Friedrich K. Tribology of Nanocomposites. *Materials Forming Machining & Tribology*, 2012.

11. Liu FB, Li HP, Cui Y, Di JJ, Qu M, Sun QG. Tribological Behavior of Ion Implanted AISI 440C Stainless Steel under Oil Lubricated Condition. *Applied Mechanics & Materials*. 2013;419:334-340.

12. Mello CB, Ueda M, Lepienski CM, Reuther H. Tribological changes on SS304 stainless steel induced by nitrogen plasma immersion ion implantation with and without auxiliary heating. *Applied Surface Science*. 2009;256(5):1461-1465.

13. Wang Z, Gao D. Friction and wear properties of stainless steel sliding against polyetheretherketone and carbon-fiber-reinforced polyetheretherketone under natural seawater lubrication. *Materials & Design*. 2014;53:881-887.

14. Yousif BF. Adhesive Wear Characteristics of Natural Fiber-Reinforced Composites. In: Davim JP, ed. *Wear of Advanced Materials*. Hoboken: Wiley; 2013.

15. Ueda M, Silva MM, Otani C, Reuther H, Yatsuzuka M, Lepienski CM, et al. Improvement of tribological properties of Ti6Al4V by nitrogen plasma immersion ion implantation. *Surface and Coatings Technology*. 2003;169-170:408-410.

16. Kumar N, Kataria S, Dash S, Srivastava SK, Das CR, Chandramohan P, et al. Tribological properties of nitrogen ion implanted steel. *Wear*. 2012;274-275:60-67.

17. Foerster CE, Serbena FC, da Silva SLR, Lepienski CM, Siqueira CJM, Ueda M. Mechanical and tribological properties of AISI 304 stainless steel nitrided by glow discharge compared to ion implantation and plasma immersion ion implantation. *Nuclear Instruments and Methods in Physics Research Section B: Beam Interactions with Materials and Atoms*. 2007;257(1-2):732-736.

18. Bezzazi M, Khamlichi A, Jabbouri A, Reis P, Davim JP. Experimental characterization of frictional behaviour of clutch facings using Pin-on-disk machine. *Materials & Design*. 2007;28(7):2148-2153.

19. Spigarelli S, Methedi ME, Cabibbo M. Constitutive analysis of high-temperature workability of a high-nitrogen bearing steel. *Materials Science and Technology*. 2016;32(11):1071-1078.

20. He Q, Li A, Shen Y, Li L, Li Z, Pan B. Design and application on experimental platform for high-speed bearing with grease lubrication. *Advances in Mechanical Engineering*. 2015;7(12):168-183.

21. Zhong H, Dai L, Yue Y, Wang B, Zhang X, Tan C, et al. Tribological properties of plasma-nitrided AISI 4340 steel in vacuum. *Materials Science and Technology*. 2016;32(4):275-281.

22. Alpas AT, Zhang J. Effect of SiC particulate reinforcement on the dry sliding wear of aluminium-silicon alloys (A356). *Wear*. 1992;155(1):83-104.

23. Alpas AT, Embury JD. Sliding and abrasive wear behaviour of an aluminum (2014)-SiC particle reinforced composite. *Scripta Metallurgica et Materialia*. 1990;24(5):931-935.

24. Jasim KM, Dwarakadasa ES. Wear in Al-Si alloys under dry sliding conditions. *Wear*. 1987;119(1):119-130.

25. Costa HL, Hutchings IM. Hydrodynamic lubrication of textured steel surfaces under reciprocating sliding conditions. *Tribology International*. 2007;40(8):1227-1238.

26. Ma Y, Wang H, Xiao Y, Fan X, Tong J, Guo L, et al. Friction and wear behaviour of steel with bionic non-smooth surfaces during sliding. *Materials Science and Technology*. 2016;32(4):257-265.

27. Sun Y, Bell T. Sliding wear characteristics of low temperature plasma nitrided 316 austenitic stainless steel. *Wear*. 1998;218(1):34-42.

28. Jin K, Qiao Z, Zhu S, Cheng J, Bing Y, Yang J. Friction and wear properties and mechanism of bronze-Cr-Ag composites under dry-sliding conditions. *Tribology International*. 2016;96:132-140.